Supporting Information

Stacking-dependent interlayer coupling in trilayer MoS_2 with broken inversion symmetry

*Jiaxu Yan[1#], Juan Xia[1#], Xingli Wang[2], Lei Liu[3], Jer-Lai Kuo[4], Beng Kang Tay[2], Shoushun Chen[5], Wu Zhou[6], Zheng Liu[2,7] and Ze Xiang Shen[1,8]**

[1]Division of Physics and Applied Physics, School of Physical and Mathematical Sciences, Nanyang Technological University, Singapore 637371, Singapore

[2]NOVITAS, Nanoelectronics Centre of Excellence, School of Electrical and Electronic Engineering, Nanyang Technological University, Singapore 639798, Singapore

[3]State Key Laboratory of Luminescence and Applications, Changchun Institute of Optics, Fine Mechanics and Physics, Chinese Academy of Sciences, Changchun 130033, P. R. China

[4]Institute of Atomic and Molecular Sciences, Academia Sinica, Taipei 10617, Taiwan

[5]School of Electrical and Electronic Engineering, Nanyang Technological University, Singapore 639798, Singapore

[6]Materials Science and Technology Division, Oak Ridge National Laboratory, Oak Ridge, Tennessee 37831, USA

[7]School of Materials Science and Engineering, Nanyang Technological University, Singapore 639798, Singapore

[8]Centre for Disruptive Photonic Technologies, Nanyang Technological University, Singapore 637371, Singapore

1. The role of van der Waals interaction in the first-principles calculations

We calculated the interlayer binding energies using three approaches for treating the vdW interaction: LDA, GGA-PBE, and van der Waals density functionals (vdW-DF) to evaluate the accuracy of our results. As shown in Fig. S1, the LDA and vdW-DF exhibit similar tendency in describing the interlayer binding, whereas the GGA-PBE predicts much less binding. Moreover, apart from the GGA-PBE data, both LDA and vdW-DF results are in excellent agreement with the experimental cell parameters. We also compared the relative ground-state total energies with respect to the most stable stacking order in Fig. S2 obtained by using LDA and vdW-DF. Obviously, the two methods correctly predict the AB stacking (2H phase) as the most favorable phase and deliver the same stability sequence.

Therefore, our results indicate that the LDA yields comparable results with the vdW-DF for MoS_2 and the LDA can provide a reasonable description for the van der Waals interaction [1-3].

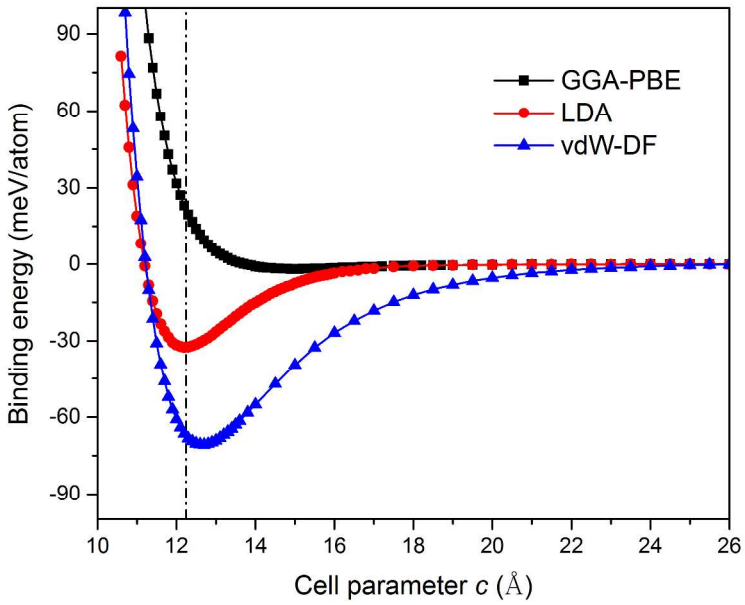

Figure S1 Calculated binding energies as a function of cell parameter *c* in 2H-MoS2, while fixing the in-plane cell parameter *a* at the bulk value. The experimental value of *c* axis is indicated by the vertical line [4].

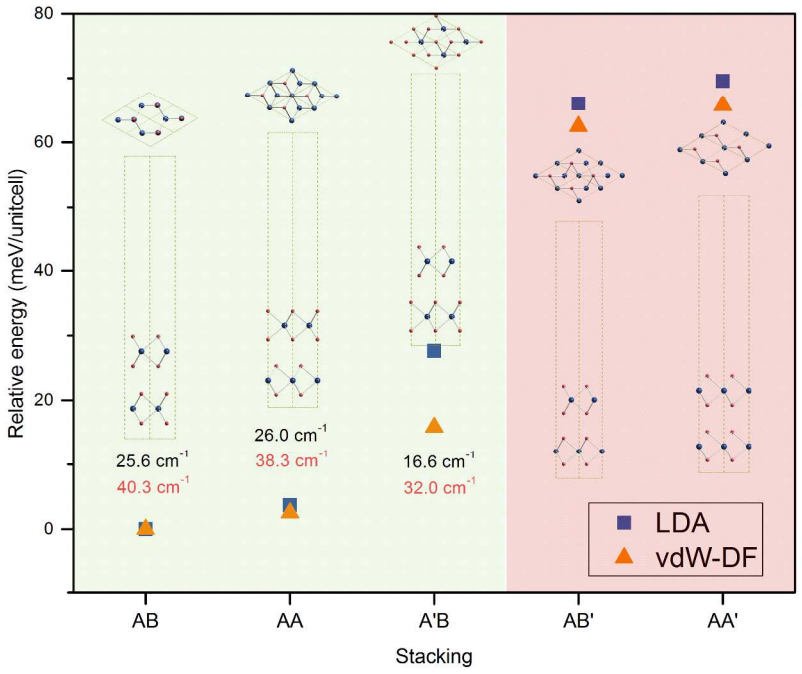

Figure S2 Relative ground-state total energies with respect to the most stable stacking order of bilayer MoS_2 (2H phase) with five possible stackings obtained by LDA and vdW-DF, as well as the corresponding ultra-low-frequency Raman shift.

2. Few-layer MoS_2 sample preparation

As for the sample preparation, we used the physical vapour deposition (PVD) technique to grow few-layer MoS_2 samples, by which we obtain a large amount of multilayer MoS_2 with various stacking configurations on the same SiO_2/Si substrate. The morphology, stacking sequence and the number of layers of our samples cannot be controlled (Fig. S3). The samples used were randomly selected.

In order to understand the growth behaviors of MoS_2, we calculated the adhesion energies of few-layer MoS_2. Starting with a monolayer MoS_2, we added one more layer each time and explored all the possible configurations. As shown in Fig. S4, we can make the following remarks: At the initial stage of MoS_2 CVD growth, MoS_2 can adopt various stacking configurations due to the comparable adhesion energies. This is the reason we obtain a large amount of few-layer MoS_2 with various stacking patterns on the same SiO_2/Si substrate.

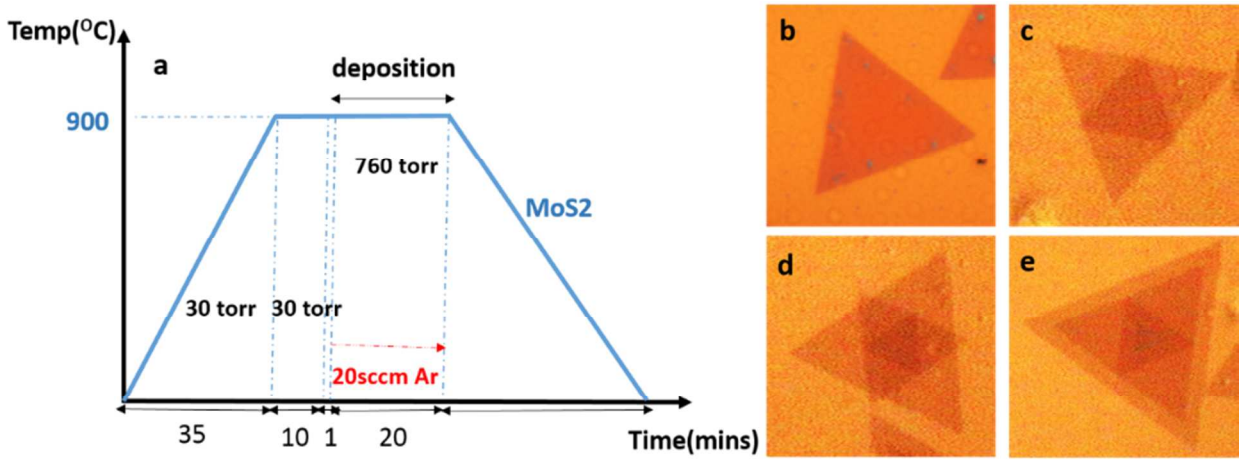

Figure S3 MoS_2 nanoflakes grown by physical vapour deposition (PVD). a The temperature ramping diagram of the whole growth process. b-d, The morphologies of as grown few-layer MoS_2 in one substrate with single layer (b), bilayer (c), trilayer (d) and quad-layer (e).

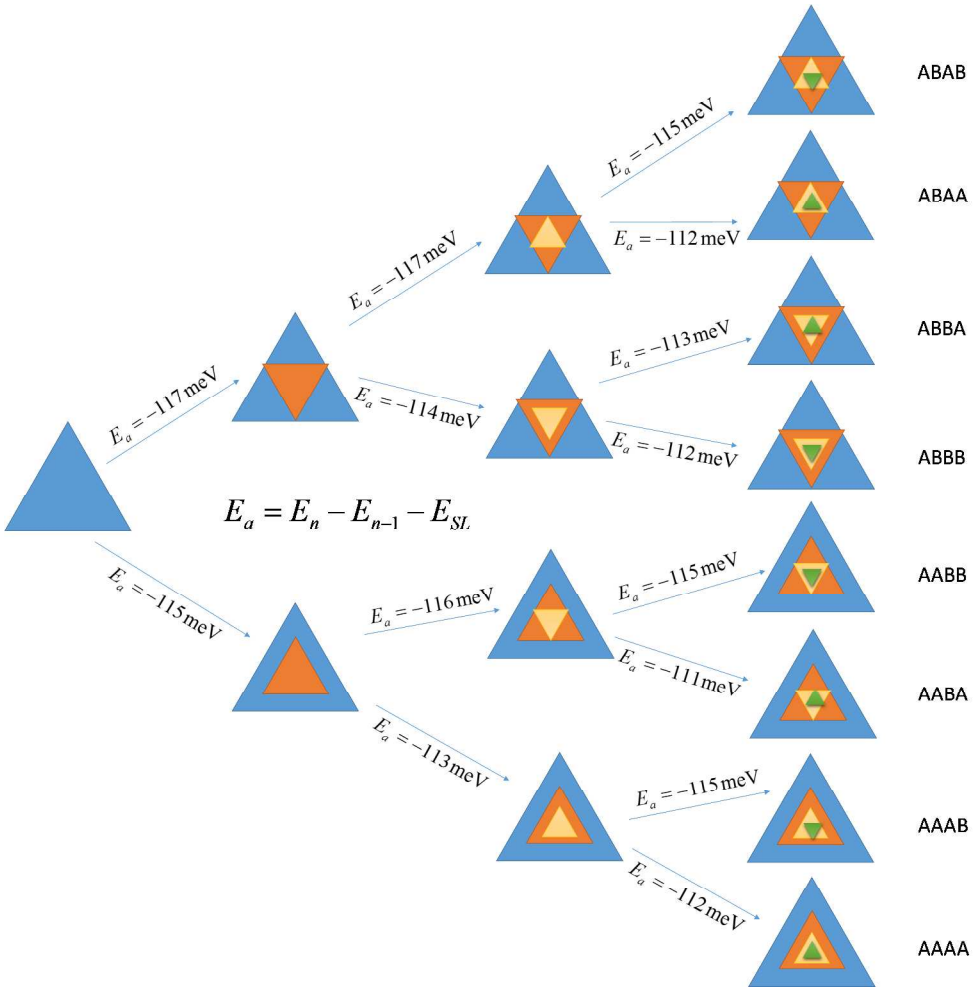

Figure S4 Calculated adhesion energies for few layer MoS_2 growth in a successive manner. The adhesion energy for the *n*th layer MoS_2 is estimated by subtractting the energy of *n-1* layer and the single layer MoS_2, as illustrated in the inset.

3. Force constants model for bilayer MoS_2

We adapted the force constants model of bulk MoS_2 [5] to our bilayer system. Given the symmetry of each mode, we can obtain following equations of force constants of bilayer MoS_2 including first- and second-nearest-neighbour interactions:

$$\omega^2(A_{2u}^2, E_{1u}^2)G = \frac{k_{12}+k_{23}+k_{24}}{m_{Mo}} + \frac{k_{23}+k_{24}}{m_S}$$

$$\frac{\omega^2(B_{2g}^1, E_{2g}^1)+\omega^2(B_{2g}^2, E_{2g}^2)}{2} G = \frac{(k_{23}+k_{24}+2k_{34})m_{Mo}+(k_{23}+k_{24}-k_{12})m_S}{2m_S m_{Mo}}$$

$$\omega^2(A_{1g}, E_{1g})G = \frac{k_{23}+k_{24}+2k_{13}+2k_{34}}{m_S}$$

$$\omega^2(B_{1u}, E_{2u})G = \frac{k_{23}+k_{24}+2k_{13}}{m_S}$$

where $G = -4\pi^2 c^2 \mu$, c is the speed of light in cm/s, μ is the unit layer mass per unit area. It is worth noting that k_{12}/k_{23} is fixed at the ratio of k_{12} in monolayer MoS_2 to that in bulk MoS_2 (~1.03).

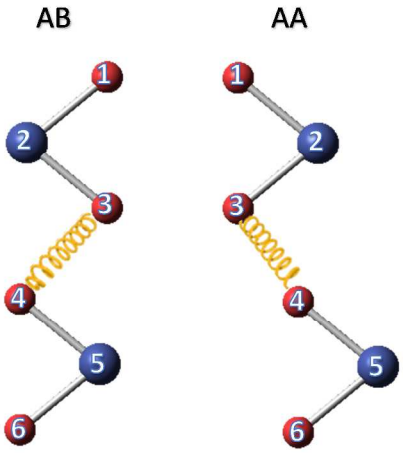

Figure S5 Lattice structures and the linear chain models of bilayer MoS_2 with AB and AA stacking. The labels on the atoms are used for constructing the notation of force constants. The weak interlayer interaction is indicated by a spring.

Table S1 Calculated parameters (in N/m^3) by fitting the force constants models to our first-principles results for AB and AA stacking bilayer MoS_2.

	k_{12}	k_{23}	k_{13}	k_{34}	k_{24}
AB stacking					
In plane	2.16×10^{21}	2.09×10^{21}	9.09×10^{20}	1.02×10^{19}	2.59×10^{19}
Out of plane	3.22×10^{21}	3.13×10^{21}	3.98×10^{20}	5.25×10^{19}	3.68×10^{19}
AA stacking					
In plane	2.16×10^{21}	2.09×10^{21}	9.04×10^{20}	0.34×10^{19}	3.38×10^{19}
Out of plane	3.22×10^{21}	3.13×10^{21}	4.02×10^{20}	7.66×10^{19}	0.43×10^{19}

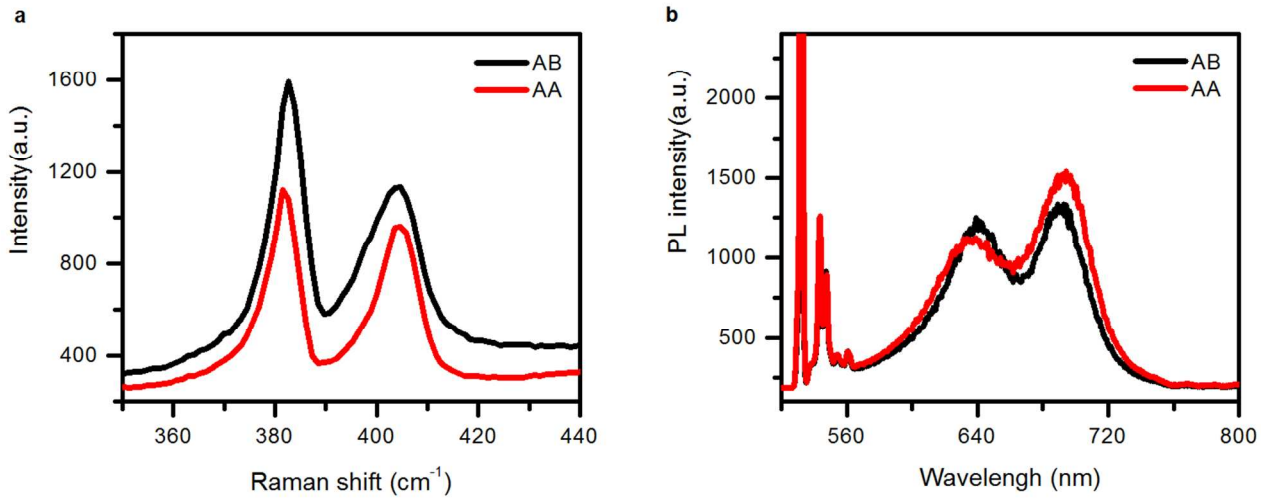

Figure S6 Raman spectra and Photoluminescence spectra of bilayer MoS_2 with AA- and AB-stacking respectively

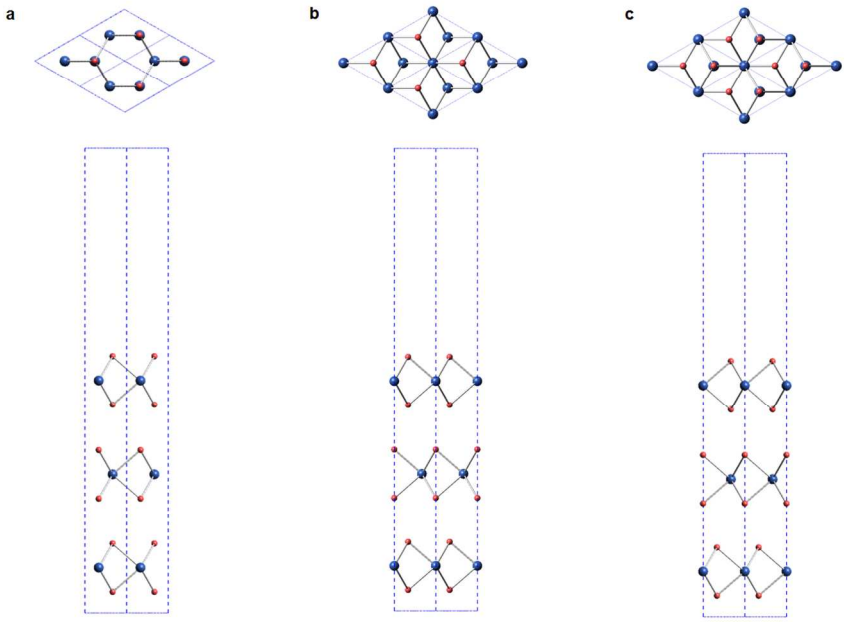

Figure S7 Top view and side view of the atomic structures of trilayer MoS_2 with ABA-, AAA- and AAB-stacking respectively.

Table S2 Calculated Gamma-point phonon frequencies of ABA-, AAA- and ABB-stacking trilayer MoS_2 respectively.

Stacking	ABA	AAA	ABB
E’’[R]	12.13	13.56	11.96
A'_1 [R]	28.47	25.78	26.73
E’[I+R]	28.58	30.49	28.32
E’[I+R]	283.77	286.41	285.56
E’[I+R]	380.86	382.44	381.89
E’’[R]	382.86	383.88	383.11
E’[I+R]	382.93	384.14	383.86
A'_1 [R]	403.72	404.86	403.87
A'_1 [R]	463.63	466.47	466.30

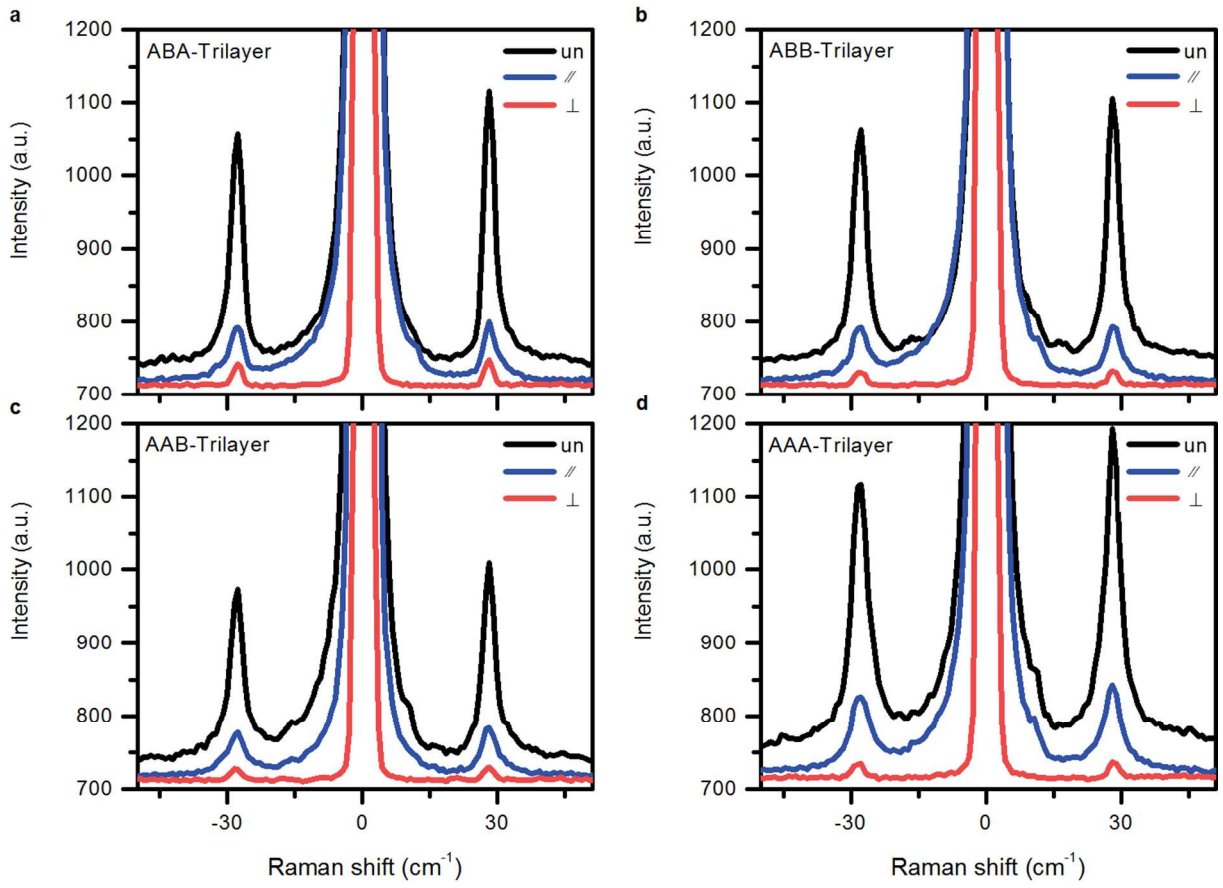

Figure S8 The low wavenumber Raman spectra of the third layer of trilayer MoS_2 samples in Figure 3**(a).** The black, blue and red curves represent the unpolarized (un) collection, $\bar{z}(xx)z$ (//) and $\bar{z}(xy)z$ (⊥) polarized configuration respectively.

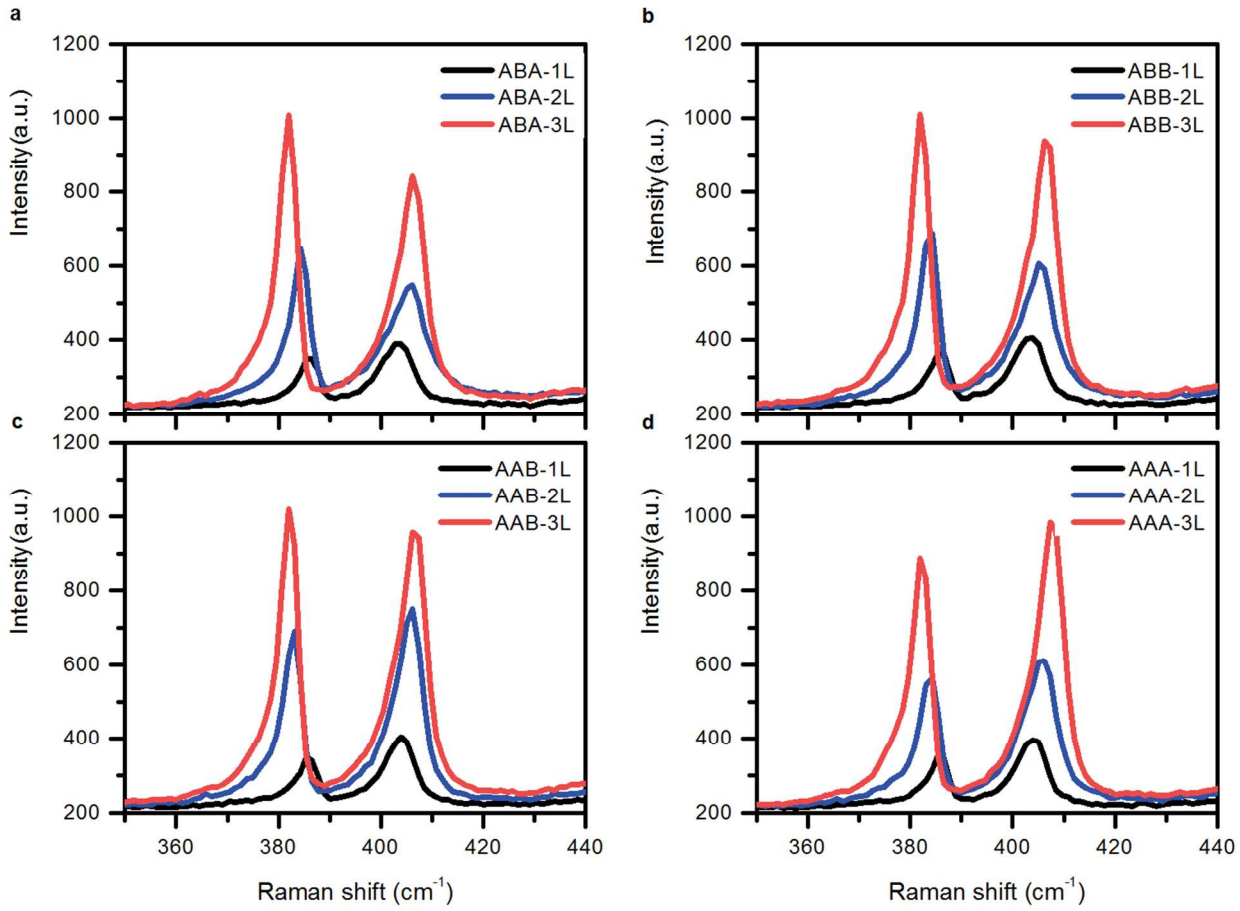

Figure S9 Raman spectra of trilayer MoS_2 samples in Figure 3**(a)** from the first layer to third layer with prominent E^1_{2g} and A_{1g} peaks representing in-plane vibration and out-of-plane vibration respectively.

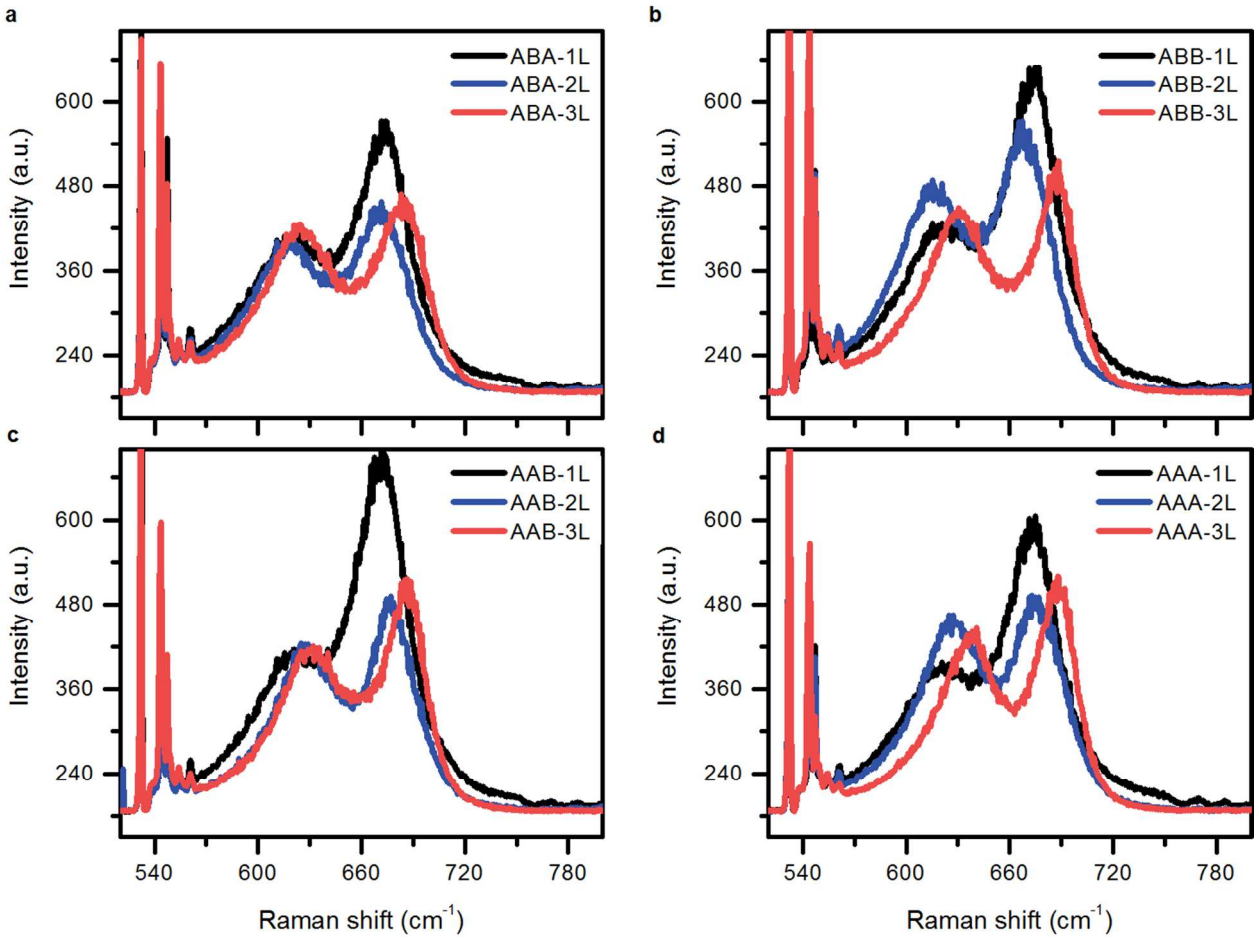

Figure S10 Photoluminescence spectra of trilayer MoS_2 from the first layer to third layer with prominent two peaks from A and B excitons respectively.

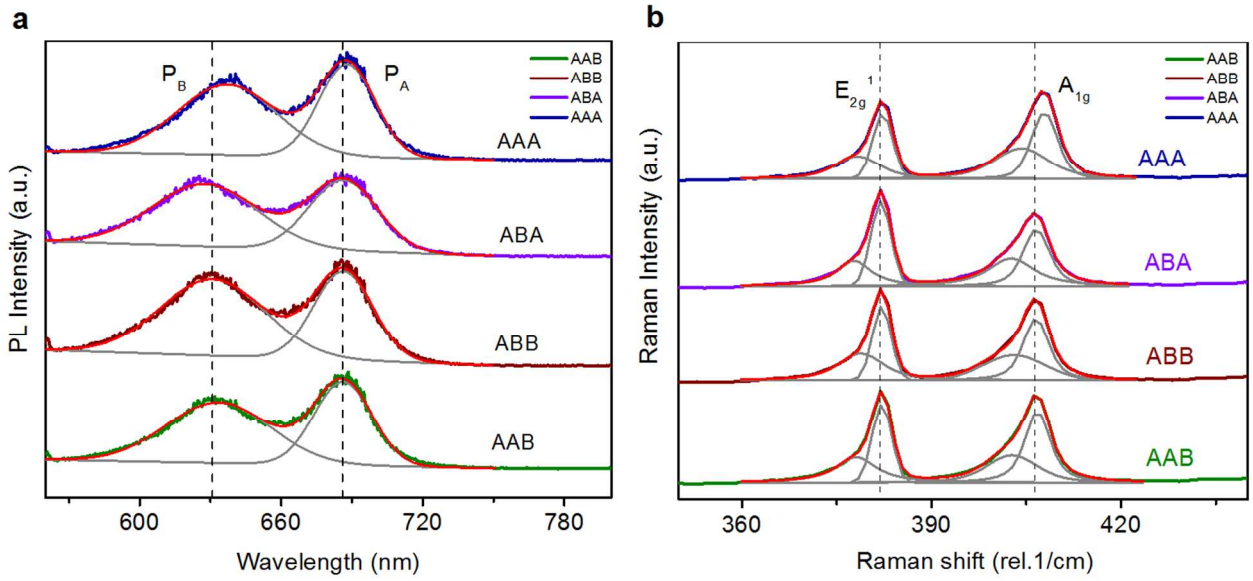

Figure S11 Fitting results of Photoluminescence spectra (Lorentz) and Raman spectra (Gauss) of trilayer MoS_2 with ABA-, ABB-, AAB-, and AAA-stacking respectively.

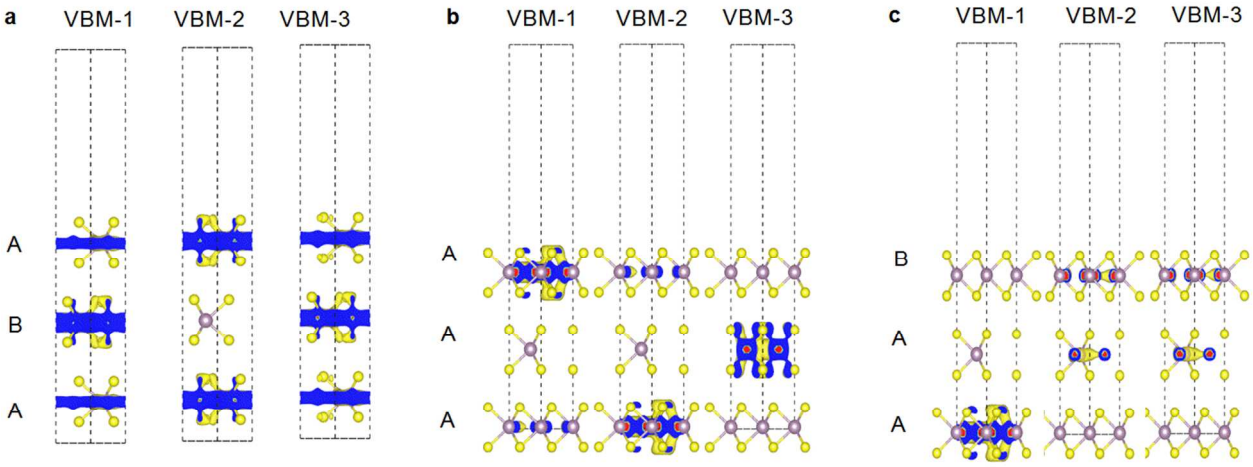

Figure S12 Stacking dependent charge density distribution of the top three valence bands of ABA-, AAA- and AAB-trilayer MoS_2.

Reference

[1] Graziano G.; Klimeš J.; Fernandez-Alonso F.; Michaelides A. *J. Phys.: Condens. Matter* 24, 424216 (2012).

[2] Mittendorfer F.; Garhofer A.; Redinger J.; Klimeš J.; Harl J.; Kresse G. *Phys. Rev. B* 84, 201401 (2011).

[3] Björkman T., Gulans A., Krasheninnikov AV., Nieminen RM. *J. Phys.: Condens. Matter* 24, 424218 (2012).

[4] Böker Th., Severin R., Müller A., Janowitz C., Manzke R., Voß D., Krüger P., Mazur A., Pollmann J. *Phys. Rev. B* 64, 235305 (2001).

[5] Luo X., Zhao Y.Y., Zhang J., Xiong Q.H., Quek S.Y. *Phys. Rev. B* 88, 075320 (2013).